

Original Research

Diagnosis of Autism Spectrum Disorder by Dynamic Local Graph-Theory Indicators Based on Electroencephalogram

Hao Luo¹, Shuo Yang¹, Nanxiang Zhang¹, Leen Huang¹, Yingfeng Ge¹, Ang Chen², Jianping Zhu³,*, Jinxin Zhang¹,*

Academic Editors: Yoshihiro Noda and Gernot Riedel

Submitted: 6 November 2023 Revised: 26 December 2023 Accepted: 11 January 2024 Published: 8 May 2024

Abstract

Background: Autism Spectrum Disorder (ASD) is a complex neurodevelopment disease characterized by impaired social and cognitive abilities. Despite its prevalence, reliable biomarkers for identifying individuals with ASD are lacking. Recent studies have suggested that alterations in the functional connectivity of the brain in ASD patients could serve as potential indicators. However, previous research focused on static functional-connectivity analysis, neglecting temporal dynamics and spatial interactions. To address this gap, our study integrated dynamic functional connectivity, local graph-theory indicators, and a feature-selection and ranking approach to identify biomarkers for ASD diagnosis. Methods: The demographic information, as well as resting and sleeping electroencephalography (EEG) data, were collected from 20 ASD patients and 25 controls. EEG data were pre-processed and segmented into five sub-bands (Delta, Theta, Alpha-1, Alpha-2, and Beta). Functional-connection matrices were created by calculating coherence, and static-node-strength indicators were determined for each channel. A sliding-window approach, with varying widths and moving steps, was used to scan the EEG series; dynamic local graph-theory indicators were computed, including mean, standard deviation, median, inter-quartile range, kurtosis, and skewness of the node strength. This resulted in 95 features (5 sub-bands × 19 channels) for each indicator. A support-vector-machine recurrence-feature-elimination method was used to identify the most discriminative feature subset. Results: The dynamic graph-theory indicators with a 3-s window width and 50% moving step achieved the highest classification performance, with an average accuracy of 95.2%. Notably, mean, median, and inter-quartile-range indicators in this condition reached 100% accuracy, with the least number of selected features. The distribution of selected features showed a preference for the frontal region and the Beta sub-band. Conclusions: A window width of 3 s and a 50% moving step emerged as optimal parameters for dynamic graph-theory analysis. Anomalies in dynamic local graph-theory indicators in the frontal lobe and Beta sub-band may serve as valuable biomarkers for diagnosing autism spectrum

Keywords: autism spectrum disorder; electroencephalography; feature extraction; dynamic functional connectivity; graph theory analysis; machine learning

1. Introduction

The complex neurological condition known as Autism Spectrum Disorder (ASD) can lead patients to exhibit repetitive and limited activities that impede their day-to-day functioning [1]. When Kanner [2] initially described ASD in 1943, he identified two key characteristics: abnormal and repetitive sensory-motor activities; and social communication impairments. Early detection and treatment could significantly mitigate the impact of later symptoms [3]. However, traditional diagnosis heavily relies on clinical-symptom questionnaires, increasing the risk of widespread misdiagnosis [4,5]. The overlapping and unclear symptoms of ASD make traditional identification challenging. Thus, it is crucial to identify biomarkers related to symptoms in order to assist in clinical diagnosis and to provide insight into the mechanisms underlying ASD [6].

Previous studies have focused on searches for fundamental biomarkers of brain functional connectivity. Because of its great temporal resolution and ease of use, electroencephalography (EEG) is typically used in these types of studies. An essential characteristic of ASD, according to electronic physiology studies, is abnormal functional neural circuits [7,8]. ASD individuals retain an excessive number of synaptic connections because they do not experience the regular pruning of synapses during childhood [9]. It has been argued that an excess of neurons creates local functional over-connectivity. The statistical dependence of signals, such as the coherence at a certain frequency, between two brain regions, over time, is referred to as functional connectivity. EEG and magnetoencephalography (MEG) can be used to determine functional connectivity. By using millisecond temporal resolution, EEG signals reflect an approximate measure of postsynaptic pyramidal cell activity

¹Department of Medical Statistics, School of Public Health, Sun Yat-sen University, 510080 Guangzhou, Guangdong, China

²Department of Science and Education, Zhongshan Bo'ai Hospital, 528400 Zhongshan, Guangdong, China

 $^{^3\}mathrm{Department}$ of Pediatrics, Zhongshan Bo'ai Hospital, 528400 Zhongshan, Guangdong, China

^{*}Correspondence: bobie 1998@hotmail.com (Jianping Zhu); zhjinx@mail.sysu.edu.cn (Jinxin Zhang)

[10]. Although some studies produced inconsistent or even contradictory results [10–13], the most widely accepted finding, currently, is that patients with ASD have lower level of long-range functional connectivity (e.g., between frontal and parietal regions) and a higher level of short-range connectivity (e.g., within frontal regions) [14]. Previous studies have mostly focused on the functional connectivity of a particular pair of regions; however, two-region connectivity is considered a low-order signal because it is considered to contain relatively little information, and cannot account for interactions from other regions [15]. In order to overcome this limitation, the topological characteristics of the entire brain functional-connection network were proposed to be described by complex network analysis, also known as graph-theory analysis [16,17].

The entire brain functional-connection network can be viewed as a graph in the graph-theory approach, with the EEG channels acting as the nodes, and the connectivity strength between channel pairs acting as the edges. An array of graph-theory indicators, which may be further classified into global and local indicators, could characterize the topological characteristics of the entire brain network. The global indicators include small-world, global efficiency, global degree, and so on, which describe the topological traits of the whole network; local indicators, such as node degree (or node strength), and node efficiency, describe the function of a specific node (or a brain region in the context of brain network) in a network [18]. Because ASD is sometimes regarded as a "disconnection syndrome", graph-theory research of brain networks is especially suitable for studying ASD [19]. Preschool-aged ASD patients showed higher node efficiency of the right lingual gyrus and a higher node degree of the right medial frontal gyrus, than did normal controls [20]. This suggests that graph-theory indicators could be useful biomarkers for the early diagnosis of ASD patients. Certain global measures, such as average node degree, are the average of their corresponding local indicators; however, the averaging process may obliterate important information necessary for diagnosis. Results suggested that there was only a significant difference in local graph-theory indicators between ASD patients and controls, not in global ones [20], which meant that some local-network topological qualities experienced modifications, and that those changes might not be discovered by global graph-theory indicators. However, it is possible to determine which features are most relevant for the disease diagnosis in a data-driven manner by fusing local graph theory with feature selection and ranking approaches [21].

Previous research tended to treat the EEG data as static. It was noted that the reason for the paradoxical results from static functional-connectivity analysis might be from not measuring instantaneous dynamic changes in EEG connectivity [22], since EEG signals are characteristically unstable. Results from a micro-state analysis showed

that EEG shifts its states in 100 ms [23]. In order to capture the dynamic characteristics of the EEG signal, a dynamic Functional-Connectivity Analysis (dFCA) was proposed. In dFCA, the EEG signal is separated into numerous epochs by a sliding window, and the variability among these epochs can be computed [24]. Functional magnetic resonance imaging (fMRI) was employed in a study of 102 normally developing control children and 105 children with ASD [25]. According to the findings, the children with ASD showed less variability in the fusiform gyrus-inferior temporal gyrus connectivity, and more variability in the anterior cingulate cortex-medial prefrontal cortex connectivity, than did the controls. Dynamic functional connectivity is useful in the identification of several illnesses, including ASD [26]. It may also reflect the dynamic reconfiguration of various regions over time, which may further reflect the brain's flexibility and adaptability. One study [23] employed the sliding-window method to divide the EEG signal of ASD patients and controls into several epochs. Then, the researchers used k-mean clustering to divide these epochs into four states. The results showed that, although static functional connectivity did not reveal the difference, the pattern of the two states was significantly different in ASD patients and controls, suggesting that useful information may be present in the process of state shift in ASD. Features from dynamic functional connectivity were found to achieve a higher classification accuracy for diagnosing ASD children, validating the special benefit of dynamic functional connectivity in diagnosing ASD patients [27]. The researchers did this by combining the dynamic functional-connectivity calculation with a multiple-kernel support vector machine model.

In the present study, we attempted to combine the benefits of dynamic functional connectivity and local graphtheory indicators. Using a data-driven method, we sought to identify the most discriminative features for ASD diagnosis by utilizing feature selection and ranking techniques. Furthermore, we attempted to assess the effectiveness of different window widths in dynamic functional-connectivity analysis to provide empirical information for the best window-width selection for subsequent studies. The workflow is depicted in Fig. 1.

2. Materials and Methods

2.1 Data Derivation

The EEG data and diagnosis details were obtained from Zhongshan Bo'ai Hospital's internal medical record system, located in Zhongshan City, China. The inclusion criteria for the ASD patient group were: (1) diagnosed as ASD according to Diagnostic and Statistical Manual of Mental Disorders-V (DSM-V) criteria; and (2) aged 1–6 years. Exclusion criteria for the ASD patients were: (1) a history of epilepsy seizures; and (2) patients who had suffered from other neurological, developmental diseases, or extra-cranial injury. Controls were selected from children



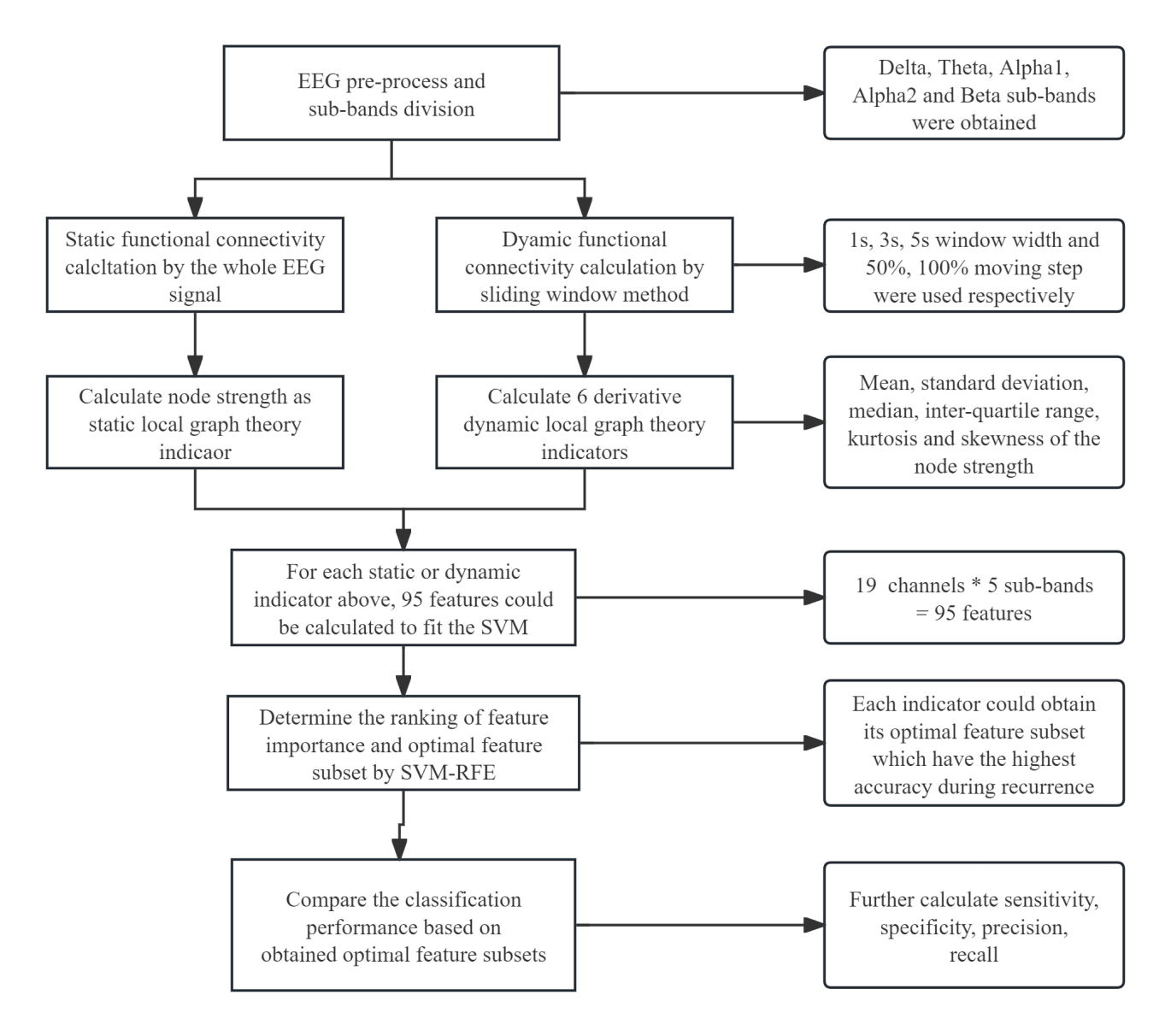


Fig. 1. The work flow of the research project. EEG, electroencephalography; SVM, support vector machine; RFE, recursive feature elimination. The * means the process of multipling. In other words, each channal could provide 5 features, and finally obtain total 95 features (19 multipling 5 equal to 95).

who were hospitalized for non-neurological disease, e.g., diarrhea, in the same age range. Altogether, 20 ASD patients and 25 health controls were recruited. Informed consent was obtained from the parents of all subjects involved in the study.

2.2 EEG Data Pre-Processing

Nicolet EEG machines (Host: PN100973M; Amplifier: V32-09472364, Natus Medical Incorporated, Pleasanton, CA, USA) with a 125-Hz sample rate were used to record the resting EEG signals of the subjects when they were sleeping. According to the international 10–20 montage system [28], a total of 19 channels (Fp1, Fp2, F7, F3, Fz, F4, F8, T3, C3, Cz, C4, T4, T5, P3, Pz, P4, T6, O1, and O2) were fastened onto the patient's scalp [29]. The

following were the EEG pre-processing steps: (1) the average re-reference and band-pass filtering between 0.1 Hz and 45 Hz were carried out for EEG signals, using the "pop_eegfiltnew" function in EEGLab toolbox v.14.1.2.0 (https://sccn.ucsd.edu/eeglab/index.php) [30] to remove artifacts; (2) independent component analysis (ICA) was carried out to remove artifacts originating from eye and muscle movement. The IClabel plug-in unit (https://labeling.ucsd.edu/auth/login) [31] carried out the identification of these components; (3) Manual elimination of the problematic segments from the eye, muscle, or body's gross movement, that ICA was unable to identify; (4) recheck, by two experts, of the pre-processed EEG data, and extraction of the 100-s signal from the beginning of the pre-processed EEG signal; and (5) EEGs were further filtered



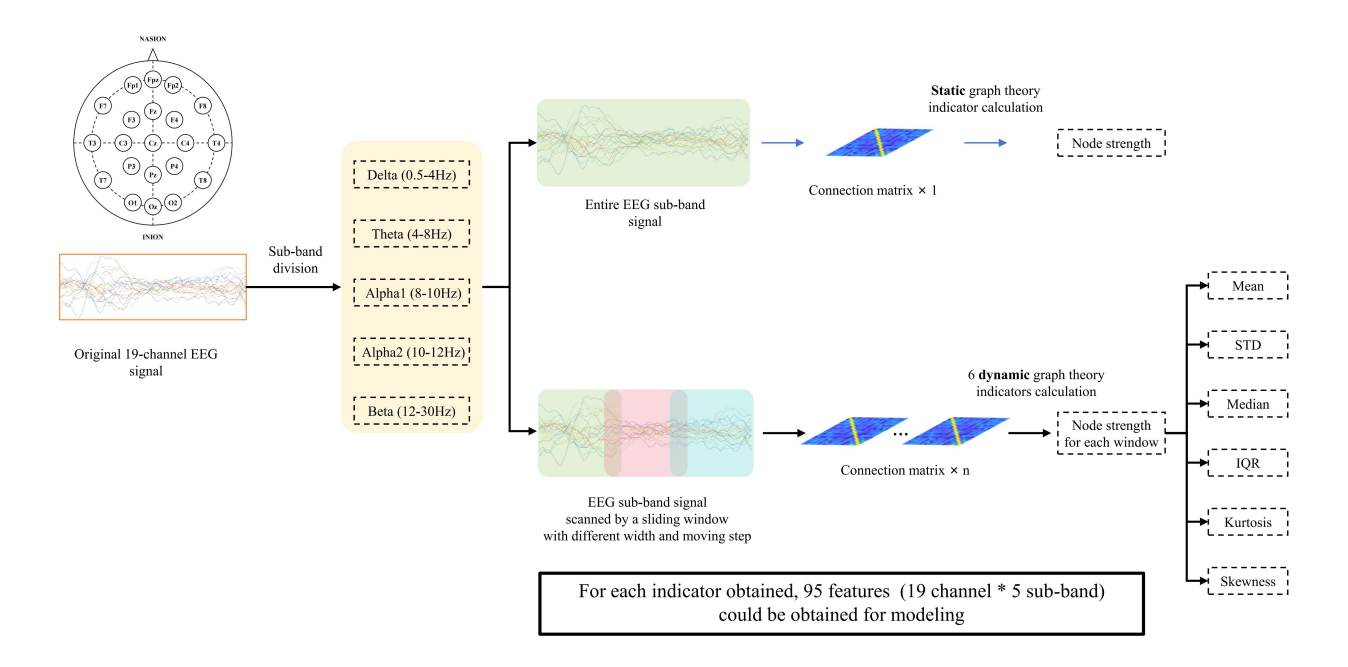


Fig. 2. The process of extracting static and dynamic graph-theory indicators. STD, standard deviation; IQR, inter-quartile range.

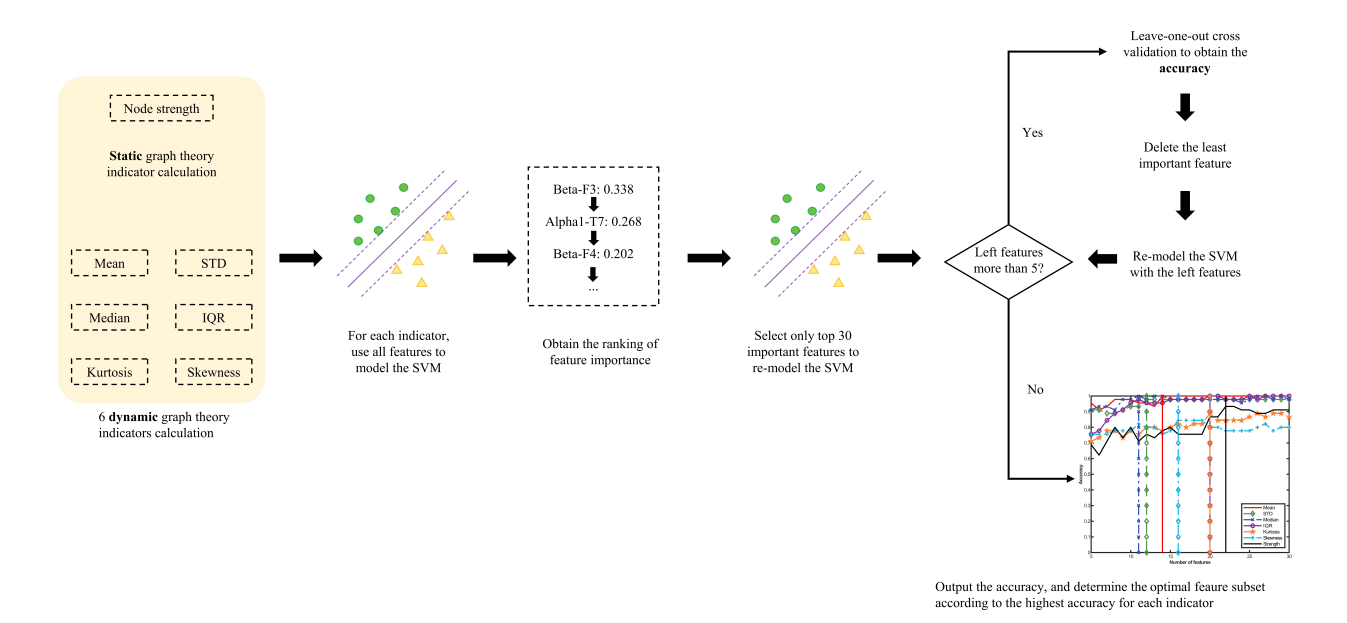


Fig. 3. The work flow of SVM-RFE.

into 5 frequency sub-bands, Delta (0.5–4 Hz), Theta (4–8 Hz), Alpha-1 (8–10 Hz), Alpha-2 (10–12 Hz), Beta (12–30 Hz) by the "pop_eegfiltnew" function in EEGLab. The pre-processing described above was carried out in Matlab v. 2019a using the EEGLab toolbox v.14.1.2.0 (https://sccn.ucsd.edu/eeglab/index.php).

2.3 Calculation of Functional Connectivity

In order to investigate the linear relationship between two signals in the fixed frequency, we computed magnitude-squared coherence, or coherence. By assuming that Y (t) and X (t) represent EEG signals in two brain regions or regions of interest (ROIs), first Y (t) and X (t) were converted from the time domain to the frequency domain using a fast Fourier transform:

$$F(f) = \sum_{t=0}^{T-1} x[t]e^{-i2\pi tf}$$
 (1)

Then, for each frequency point f, power spectral densities $S_{xx}(f)$ and $S_{yy}(f)$ and their cross power spectral den-



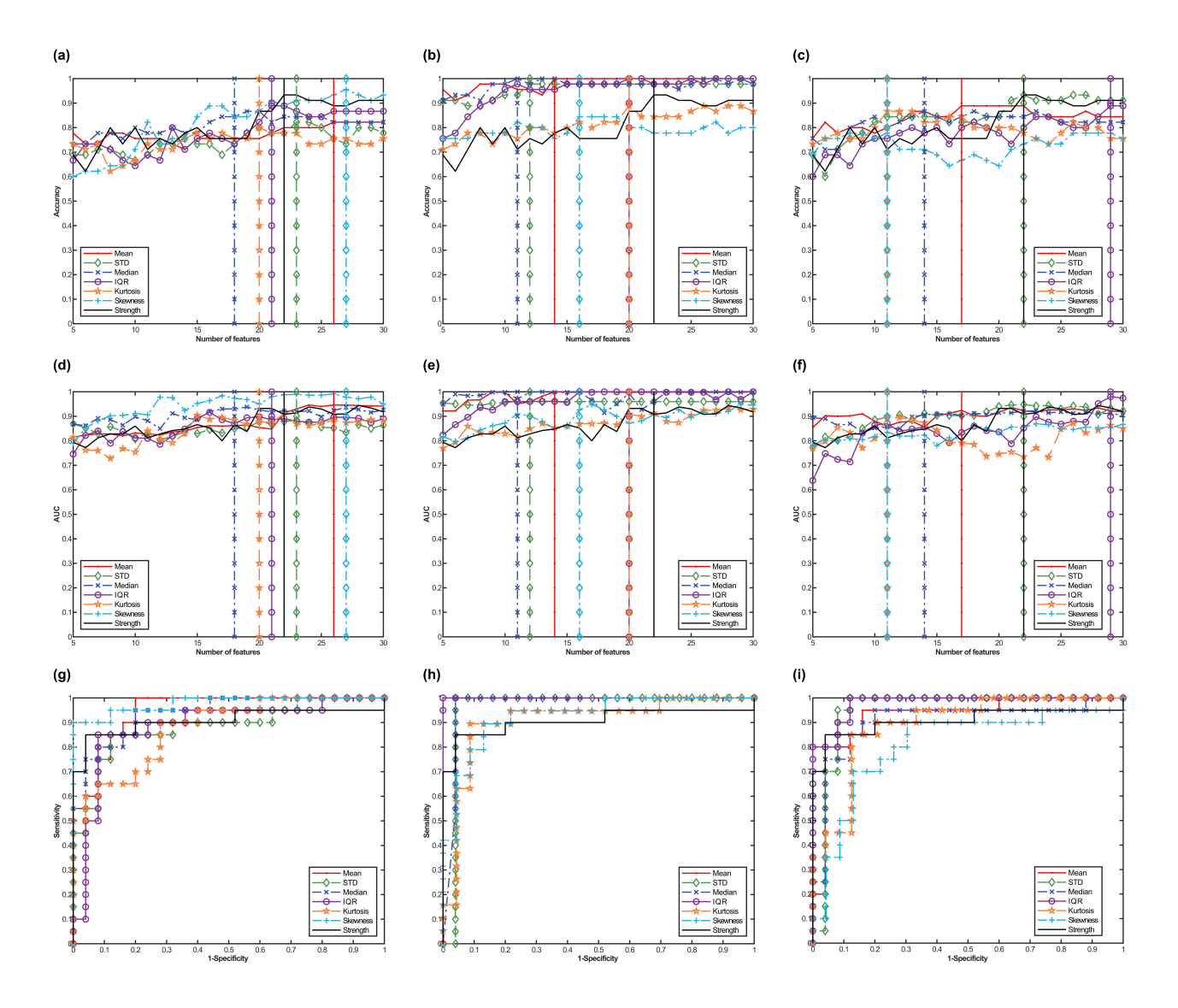


Fig. 4. The changing process of classification performance along with the recurrence and the ROC curves for the optimal feature subset in 50% moving step, and different window width conditions. (a–c) Changing process of accuracy along with the number of features under window width of 1 s, 3 s, and 5 s. (d–f) Changing process of AUC along with the number of features under window width of 1 s, 3 s, and 5 s. (g–i) The ROC based on the selected optimal feature subset under the window width of 1 s, 3 s and 5 s. The vertical line means the location where the accuracy peaks. STD, standard deviation; IQR, inter-quartile range; ROC, receiver operating characteristic; AUC, area under the curve.

sity $S_{xy}(f)$ were estimated; finally, the coherence function $K_{xy}(f)$ at that frequency point f was further calculated as follows:

$$K_{XY}(f) = \frac{S_{xy}(f)}{\sqrt{S_{xx}(f)S_{yy}(f)}}$$
 (2)

A connection matrix could be formed once all of the functional connectivity had been computed for each pair of ROIs. It is important to apply a threshold, in order to eliminate low-connectivity edges that are driven by noise. A high threshold would produce an over-sparse connection

network, whereas a low threshold would construct a regular lattice network. Determining the appropriate threshold is an arbitrary and contentious task. In light of this, we selected an intermediate criterion of 0.8, which preserved the top 20% of the graph's edges, in accordance with other research [32], to preserve this delicate balance.

2.4 Calculation of Static Graph-Theory Indicators

As in previous research [33], node strength was used in the present study as a static graph-theory metric for each ROI. The node strength, which represents a node's overall capacity to convey information throughout the network, characterizes a node's connectivity strength with all other



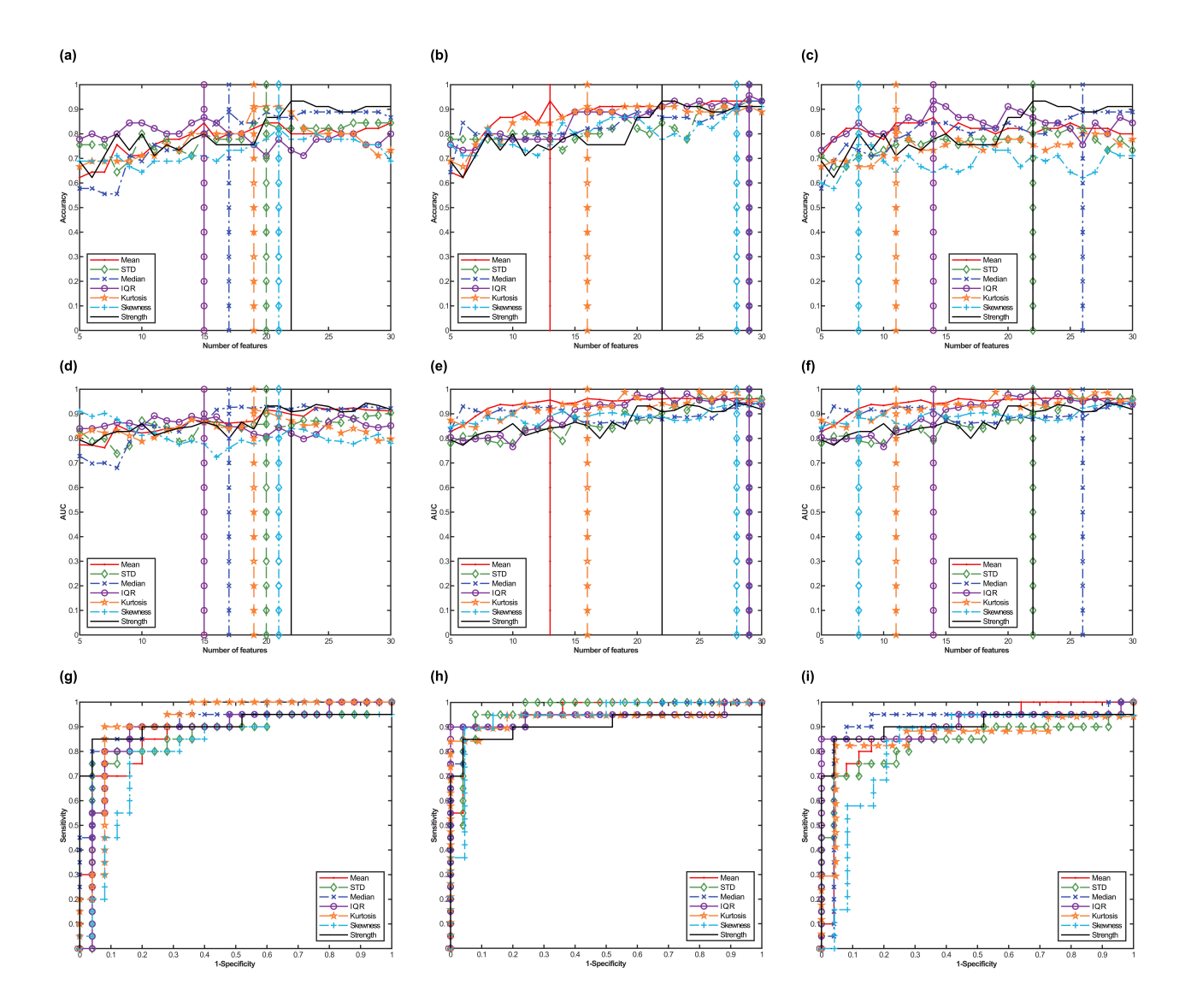


Fig. 5. The changing process of performance measures and ROC curve in 100% moving step and different window-width condition. (a–c) Changing process of accuracy along with changing of the number of features under window widths of 1 s, 3 s, and 5 s. (d–f) Changing process of AUC along with changing of the number of features under window widths of 1 s, 3 s, and 5 s. (g–i) The ROC under the window width of 1 s, 3 s and 5 s. The vertical line is the location at which the accuracy peaks.

nodes. A brain area that exhibits a high node strength is considered significant in the brain network and may be regarded as a hub of connectivity. This brain network would sustain more harm if that hub were destroyed. The examination of anomalies in the connections and interactions among different brain regions were facilitated by this indicator [34]. The following is the formula used to obtain the node strength for node I in the graph G:

$$S_{nodal}(i) = \sum_{i \neq j \in G} w_{ij} \tag{3}$$

Where the w_{ij} represents the weight of the edge linking the node j to node i.

Each subject could obtain 5 (frequency sub-band number) \times 19 (EEG channel number) = 95 features in node strength, for modeling.

All the node strengths were calculated using the "igraph" package v.1.3.5 [35] in R (v.2.3.2, Foundation for Statistical Computing, Vienna, Austria).

2.5 Calculation of Dynamic Graph-Theory Indicators

A sequence of functional-connectivity matrices can be obtained over time by using a sliding window, which can then be used to compute further dynamic graph-theory indicators. The movement step was set to be 50% or 100% of the window width, and the window width was set as 1 s, 3 s, or 5 s. We described the dynamic features along the extracted windows using six types of dynamic indicators:



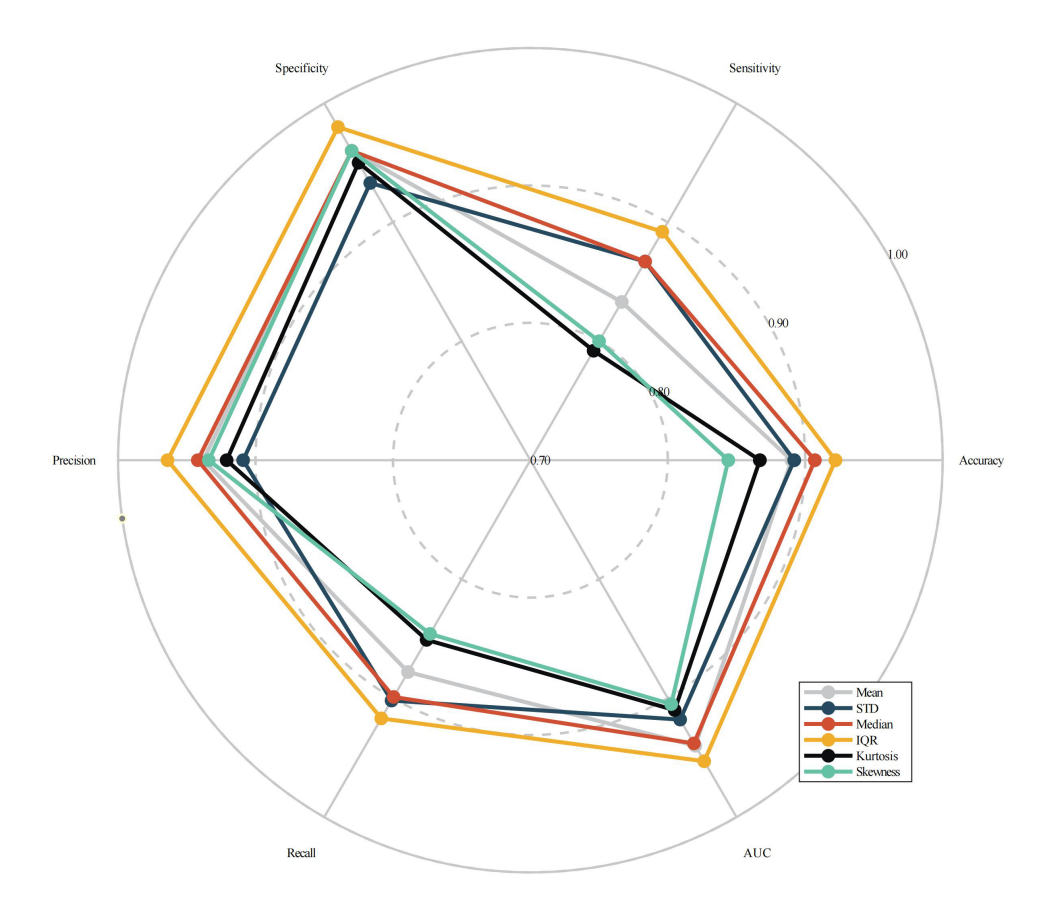


Fig. 6. The radar plot of overall performance measures across all conditions for 6 dynamic graph-theory indicators.

mean, standard deviation, median, kurtosis, inter-quartile range, and skewness of the node strength [29]. Similar to the static node-strength indicator, each subject's 5 (frequency sub-band number) \times 19 (EEG channel number) = 95 characteristics could be generated for each of the six dynamic graph-theory indicators. Fig. 2 depicts the process of feature extraction for both static and dynamic indicators.

2.6 Classification and Feature Selection by SVM-RFE

In the present study, support vector machine-recursive feature elimination (SVM-RFE) was used to conduct simultaneous feature reduction, ranking, and classification, because the number of features was greater than the number of subjects. The objective was to rank the importance of features and extract the most important ones to form the optimal feature subset.

Because of its great efficiency, SVM-RFE is a popular feature-selection method that uses the support vector machine's (SVM) classification performance as the standard [36]. SVM-RFE is a quick heuristic search approach that requires a straightforward process and relatively little computation. The feature-ranking and selection process happens nearly concurrently with model creation.

The foundation of SVM-RFE is the SVM classification algorithm, which looks for a hyperplane that fully divides samples into positive and negative classes. The sample set can be expressed as follows: The m = sample size, xi = a d-dimension vector of features, and y = the label of that sample.

$$D = \{(x_1, y_1), (x_2, y_2), \dots, (x_m, y_m)\},\$$

$$x_i \in R^d, y_i \in \{+1, -1\}$$
(4)

The hyperplane w can be formulated as:

$$w^T + b = 0 (5)$$

$$\begin{cases} w^T x_i + b \ge +1, y_i = +1 \\ w^T x_i + b \le -1, y_i = -1 \end{cases}$$
 (6)

Finally, for the *j*th feature, the importance of that feature can be calculated as the square of that coefficient in w, namely:

$$c_j = w_j^2, j = 1, 2, \dots, d$$
 (7)



After acquisition of each feature's importance and rating, the SVM-RFE was used to determine which feature subset had the best classification accuracy. The following is the process for the SVM-RFE: (1) features were arranged according to the coefficient size of each feature, as determined by formulation (7); (2) the SVM model was established, preserving all of the features, and the average accuracy of the test set was determined using leave-one-out cross-validation (LOOCV); (3) the least important feature was eliminated, and the step (2) was repeated to obtain the average accuracy on the test set, until the program reached the end condition; (4) the feature subset that had the highest average accuracy in test set was extracted. The subset with the fewest features would be chosen if the accuracy of the multiple feature subsets was the same. (5) To further characterize the classification performance for the selected feature subset, further classification measures (steps 8–12, below) would be computed. Fig. 3 depicts the SVM-RFE workflow.

$$Accuracy = \frac{TP + TN}{TP + TN + FP + FN}$$
 (8)

$$Sensitivity = \frac{TP}{TP + FN} \tag{9}$$

$$Specificity = \frac{TN}{TN + FP}$$
 (10)

$$Presicion = \frac{TP}{TP + FP} \tag{11}$$

$$Recall = \frac{TN}{TN + FN} \tag{12}$$

TP: True positive; TN: True negative; FP: False positive; FN: False negative.

We only included the top 30 significant features in the recurrence so as to minimize the amount of computation required. The least significant characteristic would be eliminated in each repetition until the subset contained just the top five significant features. SVM-RFE was run using self-edited code in Matlab v. 2019a (MathWorks, Natick, MA, USA). The SVM model was established using the "fitcsvm" function, and the parameter was left at its default value of C=1.0.

3. Results

3.1 Analysis of Demographic Data

The median age of the ASD group and the control group were 37.5 months and 32.0 months, respectively, and showed no difference ($\alpha = p \le 0.05$) according to the Wilcoxon rank-sum test (p = 0.192). The proportions of males were 20% and 28% for the ASD group and control group, respectively, which showed no difference by Fisher's exact probability test (p = 0.730). Of 20 ASD children, 19 reported an Aberrant Behavior Checklist (ABC) total score; the median was 88 (83.50, 118.5).

3.2 Comparison of Classification Performance with Different Window Widths and Moving Steps

Table 1 displays the performance metrics for the static node strength and its six derivative dynamic local graphtheory indicators, under window-width conditions of 1 s, 3 s, and 5 s, with a 50% moving step. Table 2 presents the results of a significance test conducted using the Wilcoxon signed rank test to compare the accuracy and number of selected features of average dynamic graph theory with its static counterpart. Fig. 4 depicts the changing process of accuracy and area under the curve (AUC) along with changing of the number of features, and the Receiver Operating Characteristic (ROC) curve for the optimal feature subset.

According to Tables 1,2 data, the average classification accuracy of dynamic graph-theory indicators, under window widths of 1 and 5 s, was 0.859 and 0.870, respectively, and was lower than that of the static equivalent, 0.933. When the width was 3 s, however, the average accuracy was 0.952, which was greater than the static counterpart (0.933). Among the indicators, the mean, median, and inter-quartile range of node strength even reached the accuracy and AUC equal to 1.000. The significance test for the average accuracy of these 6 dynamic indicators in 3-s windows indicated that there were no significant differences with their static equivalents (p = 0.525). This may have been because the kurtosis and skewness indicators showed comparably lower classification accuracy (0.889 and 0.844, respectively). But as we could see, in the selected optimal feature subset, 6 dynamic indicators required an average of 15.5 features in the 3-s window-width condition. This was the lowest number of features required, compared to the 1-s (22.5) and 5-s (17.3) window-width conditions, and it was also significantly lower than the number of features required in the static condition (22, p = 0.036).

Fig. 4 shows the classification performance for six different types of dynamic indicators, represented by broken lines of different colors. The black line represents the static node strength indicator, and the vertical line indicates the location where this indicator reached its maximum accuracy. Regardless of the number of characteristics (X-axis), we can observe that the accuracy of the red line (Mean), green line (STD), dark blue line (Median), and purple line (IQR) was typically higher than that of the black line un-



Table 1. Performance measures for static node strength indicator and its 6 derivative dynamic graph theory indicators under moving step as 50%.

	0. 4							
Type of indicator	Name of indicator	Accuracy	Sensitivity	Specificity	Precision	Recall	AUC	Number of features
								in optimal subset
Static	Strength	0.933	0.8500	1.000	1.000	0.893	0.944	22
	Mean	0.822	0.700	0.920	0.875	0.793	0.946	26
	STD	0.822	0.750	0.920	0.875	0.808	0.884	23
1 s window width an	Median	0.867	0.800	0.920	0.889	0.852	0.938	18
50% moving step	IQR	0.889	0.850	0.960	0.917	0.885	0.916	21
	Kurtosis	0.800	0.650	0.920	0.867	0.767	0.910	20
	Skewness	0.956	0.900	1.000	1.000	0.926	0.992	27
	Average	0.859	0.775	0.940	0.904	0.839	0.931	22.5
	Mean	1.000	1.000	1.000	1.000	1.000	1.000	14
	STD	0.978	1.000	0.960	0.952	1.000	0.960	12
2 : 1 : 141	Median	1.000	1.000	1.000	1.000	1.000	1.000	11
3 s window width and	a IQR	1.000	1.000	1.000	1.000	1.000	1.000	20
50% moving step	Kurtosis	0.889	0.850	1.000	1.000	0.885	0.934	20
	Skewness	0.844	0.800	1.000	1.000	0.840	0.950	16
	Average	0.952	0.942	0.993	0.992	0.954	0.974	15.5
	Mean	0.889	0.800	0.960	0.941	0.857	0.936	17
	STD	0.933	1.000	0.920	0.905	1.000	0.948	22
5 s window width an	Median	0.867	0.800	0.960	0.934	0.852	0.922	14
	a IQR	0.889	0.800	1.000	1.000	0.857	0.980	29
50% moving step	Kurtosis	0.867	0.850	0.900	0.8824	0.880	0.896	11
	Skewness	0.778	0.700	0.920	0.8571	0.778	0.870	11
	Average	0.870	0.825	0.943	0.920	0.871	0.925	17.3

STD, standard deviation; IQR, inter-quartile range; AUC, area under the curve.

Table 2. Results of Wilcoxon signed rank test for the average accuracy and number of selected features between static and dynamic conditions when the moving step is 50%.

Window w	idth Static accuracy	Average dynamic accuracy	p	Static number of features	Average dynamic number of features	p
1 s	0.933	0.859	0.059	22	22.5	0.999
3 s	0.933	0.952	0.525	22	15.5	0.036*
5 s	0.933	0.870	0.057	22	17.3	0.176

* means p < 0.05.

der the 3-s window-width condition. However, the vertical lines of the six dynamic indicators were all positioned to the left of the black vertical line, indicating that these indicators could achieve the best accuracy with the fewest features. Fig. 4g—i depicts the ROC based on the optimal-feature subset selected, and we can see that the ROC of 6 dynamic graph-theory indicators were higher than the black ROC line in the 3-s window-width condition. In the 1-s and 5-s window-width conditions, we could not see the advantages for 6 dynamic graph-theory indicators, because the colored lines crossed the black line, and were not always higher than the black line.

The above analytical process was repeated under the condition of 100% moving step, which meant that there was no overlap between two adjacent windows. The results are displayed in Tables 3,4, and Fig. 5.

Table 3 shows that although all conditions were below the static condition accuracy (0.933), the average accuracy

of dynamic graph-theory indicators under the 3-s window width remained the greatest (0.930) when compared to the 1-s (0.863) and 5-s (0.851) conditions. The average accuracy in 1-s window width was significantly lower than its static counterpart (p = 0.036), whereas the number of selected features was higher than that in static condition (p = 0.036) (Table 4).

Fig. 5 shows that, in most cases, the accuracy and AUC of the mean (red line) and kurtosis (orange line) were slightly higher than the static node strength (black line) under the 3-s window width condition. However, under the 1-s and 5-s window-width conditions, we were unable to discern any clear advantages of the dynamic indicators over their static counterparts.

Table 5 and Fig. 6 generalized the overall classification ability measures across all scenarios in order to compare the classification abilities of the six dynamic graphtheory indicators. Tables 5,6 show that the IQR indicator



Table 3. Performance measures for static strength indicator and its 6 derivative dynamic graph-theory indicators under moving step of 100%.

			step or 1	00,00				
Type of indicator	Name of indicator	Accuracy	Sensitivity	Specificity	Precision	Recall	AUC	Number of features in optimal subset
Static	Strength	0.933	0.8500	1.000	1.000	0.893	0.944	22
	Mean	0.844	0.800	0.960	0.933	0.846	0.926	15
	STD	0.844	0.800	0.920	0.882	0.846	0.904	20
1 s window width and	Median	0.888	0.850	0.960	0.941	0.884	0.934	17
	IQR	0.866	0.900	0.920	0.866	0.913	0.896	15
100% moving step	Kurtosis	0.911	0.900	0.920	0.900	0.920	0.910	19
	Skewness	0.822	0.800	1.000	1.000	0.840	0.910	21
	Average	0.863	0.842	0.947	0.920	0.875	0.913	17.8
	Mean	0.933	0.900	0.960	0.947	0.923	0.964	13
	STD	0.933	0.950	0.920	0.905	0.958	0.966	29
3 s window width and	Median	0.933	0.900	0.960	0.947	0.923	0.948	29
100% moving step	IQR	0.956	0.900	1.000	1.000	0.926	0.994	29
100% moving step	Kurtosis	0.911	0.800	1.000	1.000	0.862	0.990	16
	Skewness	0.911	0.900	0.960	0.944	0.920	0.955	28
	Average	0.930	0.892	0.967	0.957	0.919	0.970	24.0
	Mean	0.866	0.800	0.960	0.933	0.851	0.866	14
	STD	0.844	0.700	0.960	0.933	0.800	0.844	22
5 s window width and	Median	0.888	0.850	0.960	0.941	0.884	0.888	26
100% moving step	IQR	0.933	0.900	1.000	1.000	0.920	0.933	14
100/0 moving step	Kurtosis	0.822	0.700	0.960	0.875	0.793	0.822	11
	Skewness	0.755	0.700	0.880	0.800	0.769	0.755	8
	Average	0.851	0.775	0.953	0.913	0.836	0.851	15.8

Table 4. Results of Wilcoxon signed rank test for the average accuracy and number of selected features between static and dynamic conditions when the moving step is 100%.

	-					
Window wi	idth Static accuracy	Average dynamic accuracy	p	Static number of features	Average dynamic number of features	p
1 s	0.933	0.863	0.036*	22	17.8	0.036*
3 s	0.933	0.930	0.052	22	24.0	0.591
5 s	0.933	0.851	0.059	22	15.8	0.104

^{*} means p < 0.05.

Table 5. Overall performance measures across all conditions for 6 dynamic indicators.

Dynamic Feature	Accuracy	Sensitivity	Specificity	Precision	Recall	AUC	Number of features in optimal subset
Mean	0.892	0.833	0.960	0.938	0.878	0.940	16.5
STD	0.892	0.867	0.933	0.909	0.902	0.918	21.3
Median	0.907	0.867	0.960	0.942	0.899	0.938	19.2
IQR	0.922	0.892	0.980	0.964	0.917	0.953	21.3
Kurtosis	0.867	0.792	0.950	0.921	0.851	0.910	16.2
Skewness	0.844	0.800	0.960	0.934	0.846	0.905	18.5

outperformed the others, with an average accuracy of 0.922. The median indicator was next, with an average accuracy of 0.907.

3.3 Feature Ranking, Selection and Visualization

The greatest results were obtained with a window width of 3 s and a movement step of 50%. Therefore, we investigated further by examining feature rankings and the distribution of particular features on scalp regions and frequency sub-bands. Table 6 presents the feature rank-

ings and weights for 6 indicators of dynamic graph theory, in this condition. Features in the Beta and Alpha2 frequency sub-bands held the bulk of the top places, indicating that features in the high-frequency sub-bands had a greater contribution to the classification of individuals with ASD. In terms of mean, median, and IQR (all three indicators achieving 100% categorization), Beta-F3, Beta-F3, and Beta-Fp1 were the most significant features.

The proportion distribution of chosen characteristics across 6 dynamic graph-theory indicators in 5 frequency



Table 6. Performance measures for 6 dynamic graph-theory indicators under the condition of 3-s window width and 50% moving step.

moving step.											
Mea	1	STD		Media	IQR		Kurtosis		Skewne	ess	
Selected	Weight	Selected	Weight	Selected	Weight	Selected	Weight	Selected	Weight	Selected	Weight
Features (n		Features (n =		Features (n =		Features (n =		Features (n =		Features (n =	
= 14)		12)		11)		20)		20)		16)	
Beta-F3	0.338	Alpha2-P8	0.631	Beta-F3	0.320	Beta-Fp1	0.977	Beta-Fz	1.841	Beta-C3	0.887
Alpha1-T7	0.268	Alpha2-Cz	0.550	Alpha1-T7	0.155	Beta-P7	0.873	Beta-Fp1	1.316	Theta-F3	0.791
Beta-F4	0.202	Alpha2-P7	0.523	Alpha2-P7	0.154	Beta-C3	0.694	Alpha2-Fp2	0.880	Alpha1-Pz	0.680
Alpha1-P7	0.159	Alpha1-F4	0.401	Alpha2-F3	0.113	Beta-O2	0.608	Beta-Fp2	0.861	Beta-Fz	0.670
Alpha2-P7	0.147	Alpha2-Fp1	0.366	Alpha1-Cz	0.111	Beta-Fz	0.526	Beta-P8	0.845	Alpha2-T8	0.530
Alpha2-T7	0.134	Beta-Fz	0.353	Beta-Cz	0.105	Beta-O1	0.480	Theta-F8	0.798	Theta-Fz	0.470
Alpha1-Cz	0.125	Theta-P8	0.307	Beta-C3	0.089	Theta-Fz	0.480	Beta-P4	0.797	Alpha2-C4	0.460
Alpha2-F3	0.116	Theta-T8	0.287	Alpha2-Cz	0.087	Alpha1-F4	0.479	Theta-C3	0.744	Alpha2-Fz	0.451
Alpha2-Cz	0.106	Alpha2-P3	0.284	Theta-O1	0.084	Alpha2-P7	0.379	Beta-P7	0.633	Theta-F7	0.411
Beta-P7	0.103	Alpha2-C3	0.278	Delta-Cz	0.083	Beta-Fp2	0.349	Delta-C3	0.567	Beta-Cz	0.385
Alpha2-T8	0.094	Alpha1-T7	0.276	Alpha1-P7	0.083	Alpha2-T8	0.339	Theta-Fz	0.560	Alpha2-P4	0.381
Alpha1-T8	0.087	Alpha2-F4	0.271	-	-	Delta-Pz	0.326	Beta-Cz	0.536	Alpha2-F3	0.352
Theta-Pz	0.073	-	-	-	-	Alpha2-P3	0.325	Alpha2-Fz	0.530	Delta-O2	0.344
Theta-O1	0.071	-	-	-	-	Alpha1-F3	0.323	Alpha1-Fp1	0.512	Theta-C4	0.342
-	-	-	-	-	-	Alpha2-F4	0.317	Theta-C4	0.331	Delta-P8	0.334
-	-	-	-	-	-	Alpha2-P8	0.314	Alpha2-P4	0.317	Theta-Pz	0.302
-	-	-	-	-	-	Beta-F8	0.302	Alpha2-F4	0.302	-	-
-	-	-	-	-	-	Alpha1-T7	0.281	Beta-C3	0.264	-	-
-	-	-	-	-	-	Alpha2-Fp2	0.279	Beta-F7	0.244	-	-
-	-	-	-	-	-	Alpha2-T7	0.252	Theta-F4	0.242	-	-

Table 7. The proportion distribution of scalp region and frequency sub-band for selected features under the condition of 3-s window width and 50% moving step.

Scalp region	Proportion (%)	Relative	Weighed	Weighed relative	Frequency	Proportion (%)	Weighed
		importance	proportion (%)	importance	sub-band		proportion (%)
Parietal lobe	26.263	0.998	24.659	0.937	Alpha-1	14.141	10.124
Frontal lobe	36.364	0.987	46.153	1.253	Alpha-2	33.333	27.298
Temporal lobe	11.111	1.056	6.9450	0.660	Beta	28.283	40.739
Occipital lobe	7.071	0.672	4.9120	0.467	Delta	6.061	4.899
Central lobe	19.192	1.215	17.331	1.097	Theta	18.182	16.939

sub-bands is provided in Table 7. The results indicated that, with an unweighted proportion of 28%, and a weighted proportion of 40%, the features from the Beta sub-band had the dominant position. Similar to this, we investigated the distribution of particular traits on 5 regions of the scalp: parietal (P3, Pz, P4, P7, P8), temporal (T4, T5), occipital (O1, and O2), central (C3, Cz, C4), frontal (Fp1, Fp2, F7, F3, Fz, F4, F8), and parietal (P3, Pz, P4, P7, P8). It was evident that the frontal-area features that were chosen had the highest weighted proportion (46.153%) and unweighted proportion (36.364%). We also determined the relative relevance for the scalp region, taking into account that each region had a different number of channels. This was done by dividing the channel proportion (k/19, where k is the number of channels in a region). For instance, the frontal region's unweighted relative relevance was 0.987, when 0.364 was divided by 7/19. Table 7 shows that, even after accounting for channel percentage, the weighted relative relevance of characteristics from the frontal region remained the highest (1.253).

4. Discussion

4.1 Influence of Different Window Widths and Moving Steps on Classification Performance

The results showed that dynamic graph-theory indicators performed best when the window width and moving step were adjusted to 3 s and 50%, respectively. Some of them actually approached 100% accuracy.

The window-width setting in dynamic functional-connectivity analysis is still debatable and mostly dependent on researchers' personal preferences. Previous research on dynamic functional connectivity demonstrated that although an excessively wide window width would obscure the information pertaining to dynamic transient shifting, an excessively small window width would raise the possibility of adding artifacts and lowering the frequency resolution [24]. Accordingly, it appears that a satisfactory compromise between frequency resolution and the capacity to capture variability was struck in the present study, since the 3-s window width yielded the maximum accuracy. The performance of the 3-s window-width dynamic graph-



theory indicators marginally declined when the moving step was set to 100%, but it was still better than the 1-s and 5-s settings, which may provide additional support for choosing 3-s as the window width.

Another benefit in terms of preventing over-fitting was that we found that the number of selected features was lowest in the 3-s window-width and 50% moving-step conditions. One suggestion has been that when there are more features than subjects, over-fitting is more likely to happen [37]. The experimental results of Guyon et al. [36] demonstrated that the SVM algorithm benefits from feature reduction, even if SVM uses regularization approaches to partially avoid the over-fitting problem. Reducing the number of characteristics in the model enhances its interpretability while also reducing the possibility of overfitting. A model with fewer features is likewise simpler, requires less storage space, takes less time to compute, and possibly improves the model's accuracy, because it contains fewer false positives. Features with higher interpretability and lower computation costs can offer a better understanding of the relationship between the input and output features, which is advantageous in situations in which resource efficiency is crucial [38,39]. In summary, the 3-s window-width and 50% moving-step conditions allowed for the best classification performance with the fewest features needed. This finding should aid future research that uses dynamic functionalconnectivity analysis regarding window-width and movingstep selection.

4.2 Comparison between 6 Dynamic Local Graph-Theory Indicators and Preference of Frontal Region and Beta-Sub-Band-Selected Features

The IQR, an indicator that characterizes the dispersion and variance of the data distribution, had the highest accuracy among the 6 dynamic graph-theory indicators. This suggests that the value representing the variability of node strength had a significant ability to differentiate ASD patients from the control group. Only dFCA showed a significant difference in the study [40], suggesting that the functional-connectivity variability described by dFCA may offer distinct temporal information. The variability of functional connectivity reflects the instability of the information-transfer process within and between regions, and the flexibility of reconfiguration of one region with remaining regions [41].

Consistent with earlier research, the distribution analysis of a subset of features revealed a clear advantage of the frontal area. The frontal region was commonly identified as the aberrant portion using EEG or fMRI data in earlier research. The medial prefrontal cortex (mPFC) was identified as a hub of dysconnectivity in a study [42] that used lag-phase synchronization to construct functional connectivity on the cortical level, using a standardized low-resolution brain electromagnetic-tomography method. The mPFC plays an important role in the social cognition pro-

cess. Similarly, several previous investigations identified aberrant functional connectivity in the default-mode network (DMN) in ASD patients [43–45]. Higher restingstate fronto-parietal-network (FPN)-DMN dynamics were linked to lower cognitive flexibility, according to one article [46]. According to Chen et al. [47], frontal-temporal connections in ASD connectivity demonstrated larger signal fluctuations. That suggested that increased variability of connection between these two regions could hinder the processing of social and cognitive information. The above results suggested that the there is an increased variability of functional connectivity between frontal region and other regions in ASD patients. However, reports of the opposite outcome also surfaced. Findings of Chen et al. [43] indicated that mPFC-insula connection variability was lower in ASD patients. Chen et al. [43] noted that the insula served as a core region of the salience network (SN), which suppresses executive function in the absence of external input, by strengthening its functional connectivity to the mPFC to preserve an internally focused state. However, in order to be alert for any modifications from the outside, the SN would sometimes alter the network configurations. Accordingly, a decreased variability in mPFC-insula connections could explain why ASD patients exhibit more internally directed cognition and respond less to the external world [43]. In summary, our findings indicated that the dynamic graphtheory indicators of node strength of the frontal region had the greatest significance in the diagnosis of ASD, suggesting that there are abnormal interactions between the frontal and other brain regions. These results may also reflect decreased and increased variability of the functional connectivity of the frontal region with other regions simultaneously, as well as an overall abnormality in the variability of topological characteristics in the frontal region.

We found that the Beta sub-band was the most significant of 5 frequency sub-bands (unweighted proportion 28.283%; weighted proportion 40.739%), indicating that high-frequency sub-bands may contain more information about the abnormality in ASD. The most significant features for mean, median, and IQR (these 3 indicators achieved 100% classification) were Beta-F3, Beta-F3, and Beta-Fp1. Beta-frequency coherence is believed to be related to cognitive and attentional functions [48,49], and typically occurs in frontal and central region. Boersma et al. [50] observed that children with ASD have connection decrease in 51 ROI pairs, mainly in the Beta frequency. Additionally, they found that patients with ASD had significantly lower clustering coefficients and whole-brain average connection strengths in the Beta band than did controls. Research has indicated that people with ASD are less likely to be able to recruit Beta-band synchronization in large-scale networks, which could be a factor in the cognitive impairments that are common in ASD [51]. When the aforementioned information was combined with the findings of our feature-selection study, it became apparent that



the aberrant variability of functional connectivity in the Beta sub-band may have the greatest impact on ASD diagnosis.

4.3 Comparison with Similar Research and Novelty of Our Research

In a previous study [52], scientists classified ASD using the SVM algorithm, based on variables derived from brain functional connectivity across various frequency subbands obtained from fMRI. The best accuracy, according to the results, was 0.792. The Slow-4 (0.027-0.073 Hz) subband was found to include the majority of the discriminative features, and they found abnormal connections between the default mode network, the fronto-parietal network, and the cingulo-opercular network. Other research [53] classified children with ASD using the SVM model and used EEG to create a functional-connectivity network by partial correlation. They obtained the maximum accuracy at 0.800. When it came to dFCA, Price and his colleagues [27] extracted features from static and dynamic functional connectivity alternately, to match the multi-kernel support vector machine (MK-SVM) algorithm, and discovered that the dynamic feature could obtain a greater accuracy (0.900). Nevertheless, these studies only used the original functional connectivity as features to fit the model, and the ranking of feature importance was not involved. In order to differentiate ASD patients from normals, one study [54] used an ensemble classification model in conjunction with the SVM-RFE, and discovered that the posterior cingulate gyrus and precuneus had the highest ranking in terms of connection. Other researchers [55] used 5 global graph-theory indicators to attain an accuracy of 0.958 in their research using graph theory for the diagnosis of ASD. Another study [21] used a feature priority ranking by computing the node degree to fit the SVM model. The default mode network demonstrated a comparatively high network degree and discriminative capacity, and they were able to get 0.958 accuracy. In contrast to the previous research, ours has the advantage of combining indicators from local graph theory, dynamic functional connectivity, and ranking of future importance, all at once. This allowed us to make use of the dynamics information from dFCA and rank the selected features to identify the most significant ones, offering a fresh viewpoint on ASD diagnosis.

4.4 Limitations

There are several limitations to our investigation. First, because a 19-channel EEG was used, source reconstruction could not be performed to find the EEG signals at the brain level. In order to improve this, we advise that future research employs EEG recording devices with greater spatial resolution in order to gather proof of convergence between fMRI and EEG. Second, the cross-sectional-data type affected the possibility of clarifying the mechanisms underlying ASD. We anticipate that future research will in-

corporate longitudinal follow-up EEG to compile data from the development track, in order to improve classification performance and to offer an alternative viewpoint for evaluating the course of the disorder. Third, there is a need for external validation and an increase in sample size. We intend to perform our study on a bigger external-validation dataset in the future.

5. Conclusions

Our research showed that dynamic local graph-theory indicators yielded the greatest classification performance and required fewer features in the optimal feature subset, when we used a 3-second window width and a 50% moving step. The outcomes of the feature-selection process demonstrated a distinct advantage for the frontal region and the Beta band. This suggested that the frontal-region dynamics underwent modifications in its functional-connectivity interactions with other regions, particularly in the Beta subband. These findings provide novel insights into exploration of biomarkers for the diagnosis of ASD.

Availability of Data and Materials

Data related to the current study are available from the corresponding author on reasonable request.

Author Contributions

JXZ and HL were responsible for conceptualization; HL was responsible for methodology; HL performed formal analysis and investigation; HL wrote the original draft; JXZ, SY, NXZ, LEH, YFG, AC and JPZ were responsible for review and editing; AC and JPZ provided resources. The algorithm concept and design of this paper were contributed by all authors. All authors also participated in the experimental evaluation. All authors contributed to editorial changes in the manuscript. All authors read and approved the final manuscript. All authors have participated sufficiently in the work and agreed to be accountable for all aspects of the work.

Ethics Approval and Consent to Participate

The study was conducted in accordance with the Declaration of Helsinki and approved by the Ethics Committee of the School of Public Health in Sun Yat-sen University (2021-No.081). Informed consent was obtained from the parents of all subjects involved in the study.

Acknowledgment

The authors would like to thank the participants of the Department of Pediatrics and the Department of Science and Education of Zhongshan Bo'ai Hospital (Zhongshan, China) for supporting the data collection of this study.



Funding

This research was funded by the Guangdong Basic and Applied Basic Research Foundation under Grand No. 2022A1515011237.

Conflict of Interest

The authors declare no conflict of interest.

References

- Thom RP, McDougle CJ. Repetitive Thoughts and Behaviors in Autism Spectrum Disorder: A Symptom-Based Framework for Novel Therapeutics. ACS Chemical Neuroscience. 2023; 14: 1007–1016.
- [2] Kanner L. Autistic disturbances of affective contact. Nervous Child. 1943; 2: 217–250.
- [3] Belcher JR. Attention deficit hyperactivity disorder in offenders and the need for early intervention. International Journal of Offender Therapy and Comparative Criminology. 2014; 58: 27–40.
- [4] Mottron L, Bzdok D. Autism spectrum heterogeneity: fact or artifact? Molecular Psychiatry. 2020; 25: 3178–3185.
- [5] Nickel RE, Huang-Storms L. Early Identification of Young Children with Autism Spectrum Disorder. Indian Journal of Pediatrics. 2017; 84: 53–60.
- [6] Uddin LQ, Dajani DR, Voorhies W, Bednarz H, Kana RK. Progress and roadblocks in the search for brain-based biomarkers of autism and attention-deficit/hyperactivity disorder. Translational Psychiatry. 2017; 7: e1218.
- [7] Haghighat H, Mirzarezaee M, Araabi BN, Khadem A. Functional Networks Abnormalities in Autism Spectrum Disorder: Age-Related Hypo and Hyper Connectivity. Brain Topography. 2021; 34: 306–322.
- [8] Tomasi D, Volkow ND. Reduced Local and Increased Long-Range Functional Connectivity of the Thalamus in Autism Spectrum Disorder. Cerebral Cortex (New York, N.Y.: 1991). 2019; 29: 573–585
- [9] Tang G, Gudsnuk K, Kuo SH, Cotrina ML, Rosoklija G, Sosunov A, et al. Loss of mTOR-dependent macroautophagy causes autistic-like synaptic pruning deficits. Neuron. 2014; 83: 1131–1143
- [10] Mohammad-Rezazadeh I, Frohlich J, Loo SK, Jeste SS. Brain connectivity in autism spectrum disorder. Current Opinion in Neurology. 2016; 29: 137–147.
- [11] Khan S, Gramfort A, Shetty NR, Kitzbichler MG, Ganesan S, Moran JM, et al. Local and long-range functional connectivity is reduced in concert in autism spectrum disorders. Proceedings of the National Academy of Sciences of the United States of America. 2013; 110: 3107–3112.
- [12] Yerys BE, Gordon EM, Abrams DN, Satterthwaite TD, Weinblatt R, Jankowski KF, et al. Default mode network segregation and social deficits in autism spectrum disorder: Evidence from non-medicated children. NeuroImage. Clinical. 2015; 9: 223–232.
- [13] Lynch CJ, Uddin LQ, Supekar K, Khouzam A, Phillips J, Menon V. Default mode network in childhood autism: posteromedial cortex heterogeneity and relationship with social deficits. Biological Psychiatry. 2013; 74: 212–219.
- [14] Milovanovic M, Grujicic R. Electroencephalography in Assessment of Autism Spectrum Disorders: A Review. Frontiers in Psychiatry. 2021; 12: 686021.
- [15] Zhao F, Chen Z, Rekik I, Lee SW, Shen D. Diagnosis of Autism Spectrum Disorder Using Central-Moment Features From Lowand High-Order Dynamic Resting-State Functional Connectiv-

- ity Networks. Frontiers in Neuroscience. 2020; 14: 258.
- [16] Bullmore E, Sporns O. Complex brain networks: graph theoretical analysis of structural and functional systems. Nature Reviews. Neuroscience. 2009; 10: 186–198.
- [17] Miraglia F, Vecchio F, Pappalettera C, Nucci L, Cotelli M, Judica E, et al. Brain Connectivity and Graph Theory Analysis in Alzheimer's and Parkinson's Disease: The Contribution of Electrophysiological Techniques. Brain Sciences. 2022; 12: 402.
- [18] Hallquist MN, Hillary FG. Graph theory approaches to functional network organization in brain disorders: A critique for a brave new small-world. Network Neuroscience (Cambridge, Mass.). 2019; 3: 1–26.
- [19] Peters JM, Taquet M, Vega C, Jeste SS, Fernández IS, Tan J, et al. Brain functional networks in syndromic and non-syndromic autism: a graph theoretical study of EEG connectivity. BMC Medicine. 2013; 11: 54.
- [20] Li X, Wang L, Qin B, Zhang Y, Zhou Z, Qin Y, et al. A Sleeping rs-fMRI Study of Preschool Children with Autism Spectrum Disorders. Current Medical Imaging. 2020; 16: 921–927.
- [21] Zhao L, Sun YK, Xue SW, Luo H, Lu XD, Zhang LH. Identifying Boys With Autism Spectrum Disorder Based on Whole-Brain Resting-State Interregional Functional Connections Using a Boruta-Based Support Vector Machine Approach. Frontiers in Neuroinformatics. 2022; 16: 761942.
- [22] Mash LE, Linke AC, Olson LA, Fishman I, Liu TT, Müller RA. Transient states of network connectivity are atypical in autism: A dynamic functional connectivity study. Human Brain Mapping. 2019; 40: 2377–2389.
- [23] Michel CM, Koenig T. EEG microstates as a tool for studying the temporal dynamics of whole-brain neuronal networks: A review. NeuroImage. 2018; 180: 577–593.
- [24] Hutchison RM, Womelsdorf T, Allen EA, Bandettini PA, Calhoun VD, Corbetta M, et al. Dynamic functional connectivity: promise, issues, and interpretations. NeuroImage. 2013; 80: 360–378.
- [25] Guo X, Duan X, Chen H, He C, Xiao J, Han S, *et al.* Altered inter- and intrahemispheric functional connectivity dynamics in autistic children. Human Brain Mapping. 2020; 41: 419–428.
- [26] Fu Z, Sui J, Turner JA, Du Y, Assaf M, Pearlson GD, *et al.* Dynamic functional network reconfiguration underlying the pathophysiology of schizophrenia and autism spectrum disorder. Human Brain Mapping. 2021; 42: 80–94.
- [27] Price T, Wee C-Y, Gao W, Shen D. Multiple-network classification of childhood autism using functional connectivity dynamics. In Medical Image Computing and Computer-Assisted Intervention MICCAI 2014 (pp. 177–184). Springer International Publishing: Cham. 2014.
- [28] Klem GH, Lüders HO, Jasper HH, Elger C. The ten-twenty electrode system of the International Federation. Electroencephalography and Clinical Neurophysiology. 1958; 10: 371–375.
- [29] Liang Z, Chen S, Zhang J. Feature Extraction of the Brain's Dynamic Complex Network Based on EEG and a Framework for Discrimination of Pediatric Epilepsy. Sensors (Basel, Switzerland). 2022; 22: 2553.
- [30] Pion-Tonachini L, Kreutz-Delgado K, Makeig S. ICLabel: An automated electroencephalographic independent component classifier, dataset, and website. NeuroImage. 2019; 198: 181– 197.
- [31] Delorme A, Makeig S. EEGLAB: an open source toolbox for analysis of single-trial EEG dynamics including independent component analysis. Journal of Neuroscience Methods. 2004; 134: 9–21
- [32] Fallahi A, Pooyan M, Lotfi N, Baniasad F, Tapak L, Mohammadi-Mobarakeh N, *et al.* Dynamic functional connectivity in temporal lobe epilepsy: a graph theoretical and machine learning approach. Neurological Sciences: Official Journal of



- the Italian Neurological Society and of the Italian Society of Clinical Neurophysiology. 2021; 42: 2379–2390.
- [33] Amiri S, Mirbagheri MM, Asadi-Pooya AA, Badragheh F, Ajam Zibadi H, Arbabi M. Brain functional connectivity in individuals with psychogenic nonepileptic seizures (PNES): An application of graph theory. Epilepsy & Behavior: E&B. 2021; 114: 107565.
- [34] Kim D, Lee JY, Jeong BC, Ahn JH, Kim JI, Lee ES, et al. Overconnectivity of the right Heschl's and inferior temporal gyrus correlates with symptom severity in preschoolers with autism spectrum disorder. Autism Research: Official Journal of the International Society for Autism Research. 2021; 14: 2314–2329.
- [35] Csardi G, Nepusz T. The igraph software package for complex network research. InterJournal, Complex Systems. 2006; 1695: 1–9
- [36] Guyon I, Weston J, Barnhill S, Vapnik V. Gene selection for cancer classification using support vector machines. Machine Learning. 2002; 46: 389–422.
- [37] Zhou ZH. Machine Learning. Tsinghua University Press: Beijing, China. 2018. (In Chinese)
- [38] Saarela M, Jauhiainen S. Comparison of feature importance measures as explanations for classification models. SN Applied Sciences. 2021; 3: 272.
- [39] Matharaarachchi S, Domaratzki M, Muthukumarana S. Minimizing features while maintaining performance in data classification problems. PeerJ. Computer Science. 2022; 8: e1081.
- [40] Li Y, Zhu Y, Nguchu BA, Wang Y, Wang H, Qiu B, et al. Dynamic Functional Connectivity Reveals Abnormal Variability and Hyper-connected Pattern in Autism Spectrum Disorder. Autism Research: Official Journal of the International Society for Autism Research. 2020; 13: 230–243.
- [41] Zhang J, Cheng W, Liu Z, Zhang K, Lei X, Yao Y, *et al.* Neural, electrophysiological and anatomical basis of brain-network variability and its characteristic changes in mental disorders. Brain: a Journal of Neurology. 2016; 139: 2307–2321.
- [42] Wantzen P, Clochon P, Doidy F, Wallois F, Mahmoudzadeh M, Desaunay P, *et al.* EEG resting-state functional connectivity: evidence for an imbalance of external/internal information integration in autism. Journal of Neurodevelopmental Disorders. 2022; 14: 47.
- [43] Chen YY, Uljarevic M, Neal J, Greening S, Yim H, Lee TH. Excessive Functional Coupling With Less Variability Between Salience and Default Mode Networks in Autism Spectrum Disorder. Biological Psychiatry. Cognitive Neuroscience and Neuroimaging. 2022; 7: 876–884.
- [44] Wang M, Wang L, Yang B, Yuan L, Wang X, Potenza MN, et al.

- Disrupted dynamic network reconfiguration of the brain functional networks of individuals with autism spectrum disorder. Brain Communications. 2022; 4: fcac177.
- [45] Bathelt J, Geurts HM. Difference in default mode network subsystems in autism across childhood and adolescence. Autism: the International Journal of Research and Practice. 2021; 25: 556–565.
- [46] Douw L, Wakeman DG, Tanaka N, Liu H, Stufflebeam SM. State-dependent variability of dynamic functional connectivity between frontoparietal and default networks relates to cognitive flexibility. Neuroscience. 2016; 339: 12–21.
- [47] Chen H, Nomi JS, Uddin LQ, Duan X, Chen H. Intrinsic functional connectivity variance and state-specific underconnectivity in autism. Human Brain Mapping. 2017; 38: 5740– 5755.
- [48] Jaime M, McMahon CM, Davidson BC, Newell LC, Mundy PC, Henderson HA. Brief Report: Reduced Temporal-Central EEG Alpha Coherence During Joint Attention Perception in Adolescents with Autism Spectrum Disorder. Journal of Autism and Developmental Disorders. 2016; 46: 1477–1489.
- [49] Pfurtscheller G, Lopes da Silva FH. Event-related EEG/MEG synchronization and desynchronization: basic principles. Clinical Neurophysiology: Official Journal of the International Federation of Clinical Neurophysiology. 1999; 110: 1842–1857.
- [50] Boersma M, Kemner C, de Reus MA, Collin G, Snijders TM, Hofman D, et al. Disrupted functional brain networks in autistic toddlers. Brain Connectivity. 2013; 3: 41–49.
- [51] Bangel KA, Batty M, Ye AX, Meaux E, Taylor MJ, Doesburg SM. Reduced beta band connectivity during number estimation in autism. NeuroImage. Clinical. 2014; 6: 202–213.
- [52] Chen H, Duan X, Liu F, Lu F, Ma X, Zhang Y, et al. Multivariate classification of autism spectrum disorder using frequency-specific resting-state functional connectivity—A multi-center study. Progress in Neuro-psychopharmacology & Biological Psychiatry. 2016; 64: 1–9.
- [53] Buckley AW, Scott R, Tyler A, Mahoney JM, Thurm A, Farmer C, et al. State-Dependent Differences in Functional Connectivity in Young Children With Autism Spectrum Disorder. EBioMedicine. 2015; 2: 1905–1915.
- [54] Sun C, Sun D, Liu ZP. Detecting autism spectrum disorder from functional magnetic resonance imaging data with an ensemble machine learning method. In 2023 5th International Conference on Intelligent Medicine and Image Processing (IMIP). New York, NY, USA. IEEE. 2023.
- [55] Alotaibi N, Maharatna K. Classification of Autism Spectrum Disorder From EEG-Based Functional Brain Connectivity Analysis. Neural Computation. 2021; 33: 1914–1941.

